

# Hyperbranched Fluoropolymer-Polydimethylsiloxane-Poly(ethylene glycol) Cross-Linked Terpolymer Networks Designed for Marine and Biomedical Applications: Heterogeneous Nontoxic Antibiofouling Surfaces

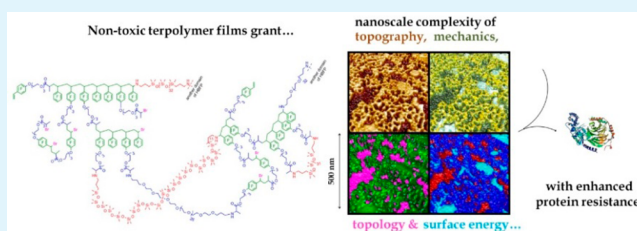
Kevin A. Pollack,<sup>†</sup> Philip M. Imbesi,<sup>†</sup> Jeffery E. Raymond,<sup>\*,†,‡</sup> and Karen L. Wooley<sup>\*,†,‡</sup>

<sup>†</sup>Department of Chemistry, Department of Chemical Engineering, Department of Materials Science & Engineering, and <sup>‡</sup>Laboratory for Synthetic-Biologic Interactions, Texas A&M University, College Station, Texas 77842-3012, United States

## S Supporting Information

**ABSTRACT:** Synthesis of terpolymer coatings composed of hyperbranched fluoropolymers cross-linked with bisamino-propyl poly(ethylene glycol) and bisamino-propyl polydimethylsiloxane (PDMS) was performed to generate antibiofouling surfaces. Nanoscale imaging and surface spectroscopy confirmed that this system possessed complex surface topographies and chemical compositions. Surface complexity was determined to be due to molecular interactions, phase segregation, and compositional gradients arising between the three components. A clear difference in surface behavior was observable before and after exposure to water. Antibiofouling characteristics were investigated by bovine serum albumin (BSA) adsorption studies; the terpolymer coating displayed a 60% greater resistance to protein adsorption in comparison to the fouling of a commercial antibiofouling silicone coating. The unique surface topography, topology, and chemical heterogeneity expressed at a variety of scales provide a robust regime for the generation of hardy, complex surfaces known to incorporate characteristics appropriate for antibiofouling applications. Thorough assessment of thermal responses and mechanical properties in relevant environments demonstrated a formulation platform immediately appropriate for consideration in marine and in vivo applications.

**KEYWORDS:** hyperbranched fluoropolymer, cross-linked networks, antibiofouling, coatings



## INTRODUCTION

Biofouling plagues a wide spectrum of applications, from medical devices to maritime vessels.<sup>1</sup> For the latter, biofouling increases the fuel consumption of the vessel, in-turn leading to increased operational and maintenance costs.<sup>1–3</sup> The conventional method of fouling prevention has been achieved through the use of toxic paints and coatings that release biocides, such as cuprous oxide and tributyltin; however, due to the negative effects that these chemicals have on the environment, the use of these systems is in decline.<sup>4,5</sup> Various combinations of polymeric materials are currently being investigated for their use as nontoxic antibiofouling coatings, applying strategies such as hydrophobicity, hydrophilicity, surface complexity, and surface energy minimization.<sup>5–18</sup>

Fluoropolymers, siloxanes, and poly(ethylene glycol) (PEG) have been researched extensively as antibiofouling agents, due to their unique chemical and physical properties.<sup>5,14–21</sup> Fluoropolymers typically possess low surface energy, low wettability and chemical stability.<sup>22</sup> In marine applications, these properties can be exploited to create coatings with increased antibiofouling performance.<sup>8,9,23–26</sup> Siloxanes, specifically poly(dimethylsiloxane) (PDMS), have shown antibiofouling characteristics, which are attributed to their low surface energy, in addition to exhibiting inertness, stability, and

pliability.<sup>1,27</sup> Commercially, PDMS coatings are marketed as nontoxic marine coatings that are capable of rejection and release of biofouling agents under suitable hydrodynamic conditions.<sup>20,27</sup> Poly(ethylene glycol) (PEG), or poly(ethylene oxide) (PEO), has been explored extensively in the field for potential marine applications, as well as in the field of biomedical engineering, because of its ability to generate surfaces that resist nonspecific protein adsorption.<sup>6,28,29</sup> Previously, combinations of these three chemical constituencies have been utilized in amphiphilic surfaces to generate an enhanced degree of antibiofouling.<sup>17</sup> However, the chemistries involved the incorporation of linear PDMS backbones, with chemical variation achieved via side group modification, where significance was placed on gaining amphiphilic character in the resultant coating. While this approach was demonstrated to be effective, we were interested in investigating topological differences of macromolecular components, their ability, in conjunction with chemical heterogeneity, to generate nano- and microscopically complex surface topographies, and the influences of these parameters in the prevention of biofouling.

**Received:** August 7, 2014

**Accepted:** October 8, 2014

**Published:** October 20, 2014

The combination of topological, topographical, and chemical heterogeneity over a variety of scales drives the development of novel coatings for the prevention of biofouling in our work. Previously, three generations of hyperbranched fluoropolymers (HBFP) were synthesized to determine the structure–property-function relationships between the fluoropolymer building blocks and ultimate network character.<sup>19</sup> Each generation of HBFP was developed to afford a polymer that, upon cross-linking with either hydrophilic or hydrophobic components, created an amphiphilic coating possessing chemical and surface heterogeneities on both the nano- and micrometer scales.<sup>30,31</sup> Related studies showed that the systems generated via cross-linking of HBFP or linear fluoropolymer with PEG moieties could be further modified by the choice of cross-linking reagent and oligomer decoration.<sup>31</sup>

This current study involves the development of novel binary and ternary amphiphilic networks through cross-linking of combinations of HBFP, PEG and PDMS. The third generation of HBFP was chosen, due to its amphiphilic character, which enhances antibiofouling performance while retaining the desired nanoscale surface heterogeneities.<sup>31</sup> The increased complexity from a third component is hypothesized to increase the antibiofouling performance when compared to the two component system of HBFP-PEG. Additionally, a terpolymer system was chosen over a system of HBFP-PDMS because of the loss of the hydrophilic PEG in that system, detracting from the potential amphiphilic properties of the resultant system. Cross-linking in this system occurred via a substitution reaction of the bromoacetyl and bromobenzyl groups of HBFP with the amine termini of both the linear PEG and PDMS cross-linkers. Deposition of a solution of the three components, followed by a thermal cure, created a thin film that was then characterized using atomic force microscopy (AFM), contact angle experiments, surface force spectroscopy, X-ray photoelectron spectroscopy (XPS), and attenuated total reflectance-infrared spectroscopy (ATR-IR). Nonspecific protein binding resistance was investigated and compared against a commercially available antibiofouling PDMS standard. Thermal and mechanical responses were determined through differential scanning calorimetry (DSC), thermogravimetric analysis (TGA), dynamic mechanical analysis (DMA), and dynamic thermal mechanical analysis (DTMA), as prepared and/or under biologically relevant conditions.

## ■ EXPERIMENTAL SECTION

**Materials.** Reagents and starting materials were purchased from Sigma-Aldrich and used as received unless otherwise noted. 2,3,4,5,6-Pentafluorostyrene (PFS) was purchased from Apollo Scientific (U.K.) and filtered through a plug of neutral alumina prior to use. 2,4,6-Tris(bromomethyl)mesitylene was purchased from Combi-Blocks. Bovine serum albumin (BSA) conjugated to Alexa Fluor 680 was purchased from Invitrogen. Sylgard 184 (Dow Corning) was purchased from Ellsworth Adhesives and was prepared as instructed.

**Nuclear Magnetic Resonance Spectroscopy and Mass Spectrometry.** Briefly, monomers and polymers were characterized by <sup>1</sup>H, <sup>13</sup>C, and <sup>19</sup>F nuclear magnetic resonance (NMR) spectroscopies using a Varian Inova 300 spectrometer. <sup>1</sup>H and <sup>13</sup>C NMR spectra were analyzed using the solvent signal as an internal reference and <sup>19</sup>F NMR spectra were analyzed with CF<sub>3</sub>COOH as an external standard. High-resolution mass spectrometry (HRMS) for the monomers was conducted on an Applied Biosystems PE SCIEX QSTAR. Spectral data for the small molecules are reported elsewhere.<sup>31</sup>

**Infrared and X-ray Photoelectron Spectroscopy.** IR spectra were obtained on a Shimadzu IR Prestige attenuated total reflectance Fourier-transform infrared spectrometer (ATR-IR). Spectra were

analyzed using IRsolution software package (Shimadzu). X-ray photoelectron spectroscopy (XPS) measurements were taken with a Kratos Axis Ultra Imaging X-ray photoelectron spectrometer, using Mono Al anode, 12 kV voltage, and 10 mA current.

**Gel Permeation Chromatography.** Gel permeation chromatography was performed on a Waters Chromatography, Inc. (Milford, MA), 1515 isocratic HPLC pump equipped with an inline degasser, a model PD2020 dual-angle (15° and 90°) light scattering detector (Precision Detectors, Inc.), a model 2414 differential refractometer (Waters, Inc.), and four PL<sub>gel</sub> polystyrene-*co*-divinylbenzene gel columns (Polymer Laboratories, Inc.) connected in series: 5 μm Guard (50 × 7.5 mm), 5 μm Mixed C (300 × 7.5 mm), 5 μm 10<sup>4</sup> (300 × 7.5 mm), and 5 μm 500 Å (300 × 7.5 mm) using the Breeze (version 3.30, Waters, Inc.) software.

**Elemental Analysis.** Elemental analysis of the polymers was performed at Midwest Microlab, LLC (Indianapolis, IN).

**Thermal Analysis.** Differential scanning calorimetric (DSC) studies were performed on a Mettler-Toledo DSC822<sup>e</sup> (Mettler-Toledo, Inc., Columbus, OH), with a heating rate of 10 °C/min. The *T*<sub>g</sub> was taken as the midpoint of the inflection tangent, upon the third heating scan. Thermogravimetric analysis was performed under Ar atmosphere using a Mettler-Toledo model TGA/DSC 1 Star<sup>e</sup> system, with a heating rate of 10 °C/min. Measurements were analyzed using Mettler-Toledo Star software version 10.00d.

**Atomic Force Microscopy and Surface Force Spectral Mapping.** Atomic force microscopy was performed under ambient conditions in air. The AFM instrumentation consisted of a MFP-3D-BIO AFM (Asylum Research; Santa Barbara, CA) and standard silicon tips (type, OTESPA-70; L, 160 μm; normal spring constant, 50 N/m; resonance frequency, 246–282 kHz). Force spectroscopy mapping was performed via AFM measurements using a Bruker Multimode 8 system in PeakForce tapping mode. This imaging method also provides direct surface maps of modulus, dispersion, deformation, and adhesion.<sup>32</sup> In brief, the PeakForce QNM imaging mode uses a modified Hertzian model, the DMT model, to directly extract a reduced Young's modulus (*E*<sub>r</sub>).<sup>24</sup> The DMT model takes into account surface-tip interactions neglected in the Hertz model and also allows for mapping of adhesion force, deformation, and dissipation energy. This method is described elsewhere in detail.<sup>31</sup>

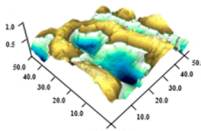
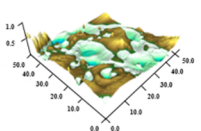
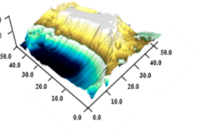
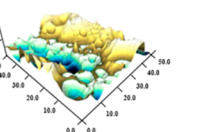
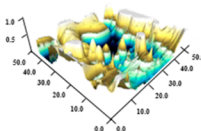
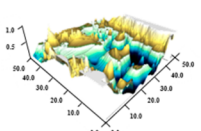
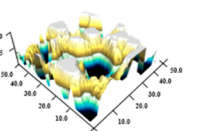
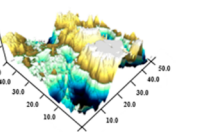
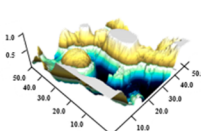
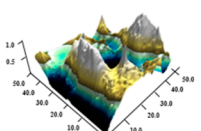
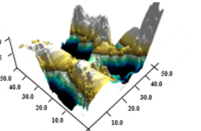
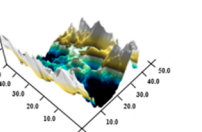
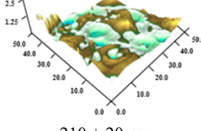
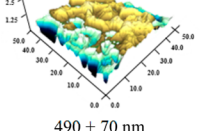
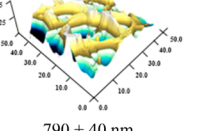
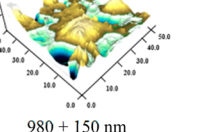
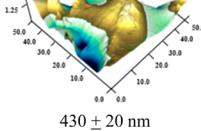
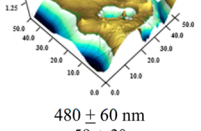
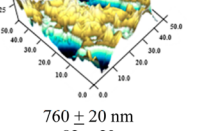
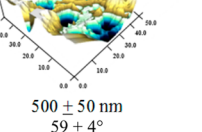
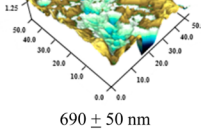
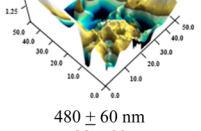
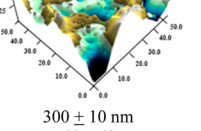
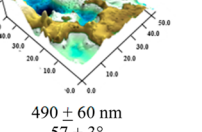
In these measurements, a ScanAsyst-Air (Bruker) with manufacturer specification for a spring constant of *k* = 0.4 was used. For this study, no formal calibration was performed as the relative values for purposes of chemical identification were sought. Arbitrary values for tip size and the Poisson ratio were used. Thermal tuning of the cantilever gave a resonant frequency of 93 kHz. However, as PeakForce imaging uses the cantilever in an off-resonance mode of 2 kHz, this finding is not critical to the qualitative value of the imaging.

**Mechanical Analysis.** A Mettler Toledo TT-DMA system was used for all dynamic mechanical and dynamic thermal mechanical analysis (DMA/DTMA) studies. Submersion studies were performed in Hyclone (Thermo) calcium/magnesium free phosphate buffered saline solution (1×, PBS) for simulation of an in vivo environment. Submersion studies were performed in synthetic seawater (Ricca Chemicals, cat. no. 8363-5, ASTM D 1141-substitute ocean water) for simulation of a marine environment. All measurements were taken in compression with a dynamic force of 0.1 N.

**Static Surface Contact Angle.** Contact angles were measured as static contact angles using the sessile drop technique with an Attension Theta optical tensiometer (Biolin Scientific).<sup>32</sup> Drops were fitted with a Young–Laplace formula to calculate the static contact angle in the Theta software (Biolin Scientific).

**Confocal Microscopy and Protein Adhesion Assay.** Bovine serum albumin conjugated to AlexaFluor-680 (BSA) was dissolved in phosphate buffered saline (PBS) solution (pH 7.1) to a concentration of 0.1 mg/mL and stored in the dark. Sylgard 184 was used as a standard to test against the terpolymer film. The surface of the terpolymer network and Sylgard 184 were incubated in fresh PBS buffer for 10 min and dried via filtered nitrogen gas. The surfaces were then exposed to Alexa-Fluor-680 conjugate in PBS at 0.1 mg mL<sup>-1</sup> for 45 min in a dark chamber. After exposure, the surfaces were washed

Table 1. Tapping Mode AFM Images of the Terpolymer Networks with RMS Roughness and Contact Angle

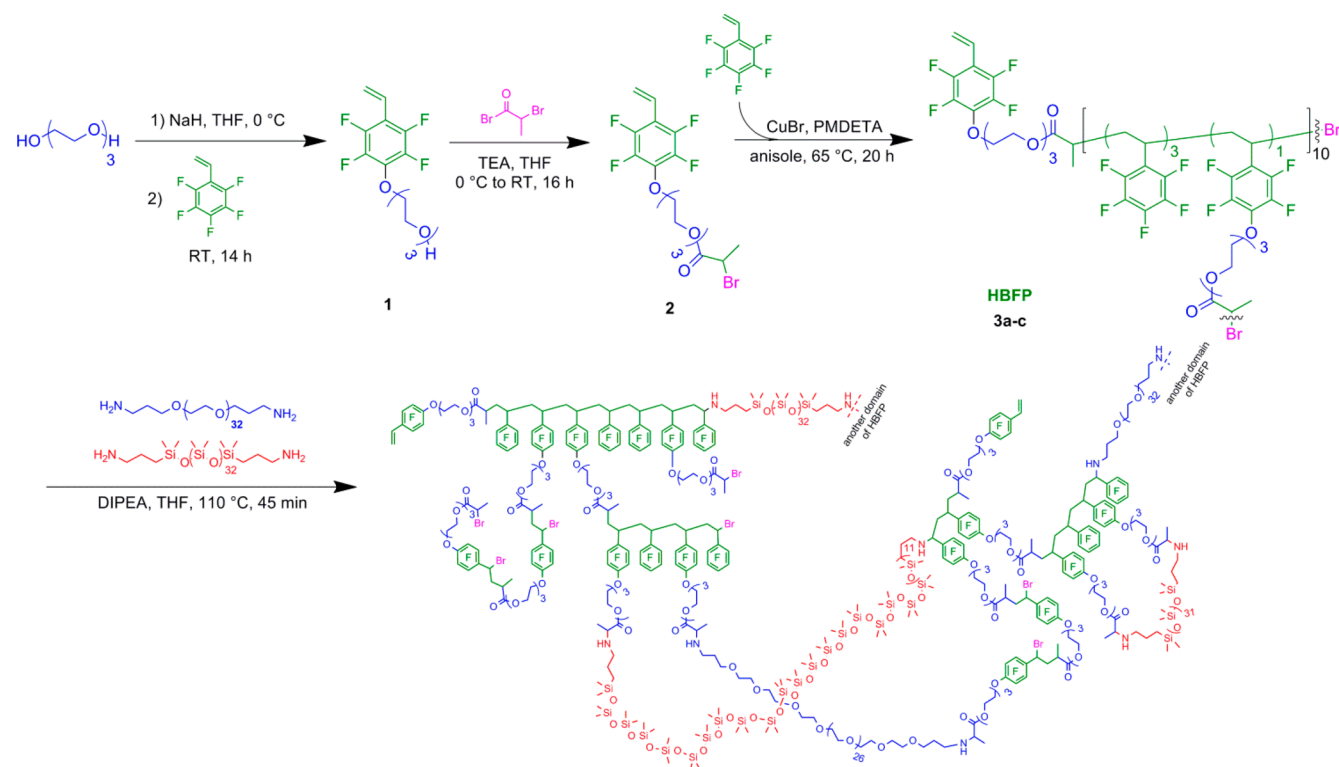
	0 wt% PEG	25 wt% PEG	50 wt% PEG	75 wt% PEG		
Pre-Swell Networks	25 wt% PDMS	 210 ± 40 nm 102 ± 3°	 360 ± 50 nm 83 ± 2°	 660 ± 120 nm 106 ± 3°	 410 ± 90 nm 107 ± 3°	
	50 wt% PDMS	 250 ± 20 nm 75 ± 3°	 420 ± 50 nm 81 ± 1°	 420 ± 120 nm 83 ± 2°	 630 ± 80 nm 78 ± 3°	
	75 wt% PDMS	 550 ± 140 nm 65 ± 4°	 590 ± 70 nm 73 ± 2°	 500 ± 90 nm 76 ± 3°	 510 ± 100 nm 75 ± 2°	
	Post-Water Immersion Networks	25 wt% PDMS	 210 ± 20 nm 106 ± 4°	 490 ± 70 nm 117 ± 3°	 790 ± 40 nm 109 ± 4°	 980 ± 150 nm 74 ± 5°
		50 wt% PDMS	 430 ± 20 nm 110 ± 4°	 480 ± 60 nm 59 ± 3°	 760 ± 20 nm 82 ± 2°	 500 ± 50 nm 59 ± 4°
		75 wt% PDMS	 690 ± 50 nm 85 ± 3°	 480 ± 60 nm 88 ± 2°	 300 ± 10 nm 65 ± 4°	 490 ± 60 nm 57 ± 3°
Field of view for dry AFM renderings is 50 μm <sup>2</sup> with a 1.0 μm z-scale. Field of view for wet AFM renderings is 50 μm <sup>2</sup> with a 2.5 μm z-scale.						

with 5 mL of PBS buffer and dried via filtered nitrogen gas for 1 h. Z-stacked confocal fluorescence images were taken of the BSA exposed surfaces and were discussed in terms of resultant intensity histograms. The imaging platform was a full spectral Olympus FV-1000 laser scanning confocal microscope operating with a 635 nm diode laser and fluorescence collection selected by a wide band monochromator from 650 to 750 nm. Depth profiles were performed that include identical step sizes and fully integrated z-stacks that are of identical depths and which included several “dead” frames both above and below the samples. No data manipulation was performed outside of z-stack integration. This protocol allowed the entirety of the surface to be collected with uniform weighting for each frame. We also imaged under identical conditions: excitation wavelength and power, optics, filters, scan rates, pixel size, collection optics, and detector voltages. Collection regimes were selected to avoid Raman interference with emission. To confirm similar laser power (e.g., to avoid a drift in laser wattage) we confirmed laser intensity by use of integrated counts at the excitation wavelength after a neutral density filter on clean glass and allowing the system to equilibrate to a power variation of <1% of total counts.

**Synthesis of Hyperbranched Fluoropolymers.** To a 250 mL Schlenk flask equipped with a stir bar was added 2 (9.00 g, 19.6 mmol), pentafluorostyrene (PFS) (11.4 g, 58.8 mmol), pentamethyldiethylenetriamine (PMDETA) (8.18 mL, 39.2 mmol), CuBr (2.81 g, 10.9 mmol), and anisole (105 mL). The solution was deoxygenated via freeze–pump–thaw (×3), the vessel was backfilled with N<sub>2</sub> and then lowered into an oil bath set at 65 °C and the reaction was allowed to proceed for 20 h. The polymerization was quenched by opening the flask to air and submerging the flask in liquid nitrogen. Once thawed, the contents were dissolved in dichloromethane (500 mL), eluted through a plug of alumina to remove the catalyst, concentrated in vacuo, and the product was isolated by precipitation into cold hexanes (3 × 1.5 L) to afford a white powder of 3 in 39% yield (7.80 g). IR = 2947, 2878, 2361, 1744, 1651, 1497, 1296, 956, and 864 cm<sup>-1</sup>. <sup>1</sup>H NMR (CDCl<sub>3</sub>, ppm): δ 0.7–1.5 (br m, C–CH<sub>3</sub>), 1.5–3.1 (br m, CH<sub>2</sub>–CH(R)– backbone), 3.4–4.0 (br m, R–O–CH<sub>2</sub>–CH<sub>2</sub>–OR'), 4.0–4.6 (br m, TFS–O–CH<sub>2</sub>–CH<sub>2</sub>–OR and R–CH<sub>2</sub>–CH<sub>2</sub>–O(O)C–R') ppm. <sup>13</sup>C NMR (CDCl<sub>3</sub>, ppm): δ 24.7, 30.7–29.7, 32.1–41.7, 63.6, 68.8, 70.0–70.8, 74.3, 114.7, 122.2, 137.6, 140.7, 144.7, 176.6 ppm. <sup>19</sup>F NMR (CDCl<sub>3</sub>, ppm): δ –143 (br m, *o*-F (PFS) and *o*-F (TFS)), –157 (br m, *p*-F (PFS) and *m*-F (TFS)), –162



Scheme 1. Synthesis of the Crosslinked HBFP-PEG-PDMS Terpolymer Films



(br m, *m*-F (PFS)) ppm. The polymerization was repeated to give several batches of HBFP: **3a**  $M_w^{\text{GPC}} = 17400$  Da,  $M_n^{\text{GPC}} = 8600$  Da,  $M_w/M_n = 1.72$ .  $T_g = 74$  °C.  $T_{\text{decomp}} = 385$  °C, 73% mass loss @ 500 °C. **3b**  $M_w^{\text{GPC}} = 20100$  Da,  $M_n^{\text{GPC}} = 11200$  Da,  $M_w/M_n = 1.79$ .  $T_g = 48$  °C.  $T_{\text{decomp}} = 385$  °C, 67% mass loss @ 500 °C. Anal. calcd for  $C_{455}H_{259}Br_7F_{238}O_{35}$ : C 48.8%; H, 2.33%; F 40.3%; Br 4.99%. Found: C 42.04; H 3.00; F 25.02; Br <0.10%. **3c**  $M_w^{\text{GPC}} = 19700$  Da,  $M_n^{\text{GPC}} = 13000$  Da,  $M_w/M_n = 1.46$ .  $T_g = 72$  °C.  $T_{\text{decomp}} = 385$  °C, 78% mass loss @ 500 °C. Anal. calcd for  $C_{534}H_{276}Br_6F_{294}O_{30}$ : C 49.3%; H 2.14%; F 42.3%; Br 3.69%. Found: C 51.05; H 3.12; F 32.12; Br 0.159%. **3a** was used for the initial AFM imaging and contact angle study, **3b** was used for the AFM data compiled in Table 1 and **3c** was used for all other studies presented.

**Design of the Hyperbranched Fluoropolymer-Poly(ethylene Glycol)-Poly(dimethylsiloxane) Cross-Linked Terpolymer Network (HBFP-PEG-PDMS) Two-Dimensional Series.** A series of HBFP-PEG-PDMS networks was prepared with a constant weight of HBFP (**3b**) and at varying wt % PEG (0–75 wt %, calculated with respect to the weight of HBFP) and PDMS (25–75 wt %, calculated with respect to the weight of HBFP) to investigate how the relative stoichiometry of the cross-linkers affected surface topography and hydrophilicity.

**General Procedure for the Preparation of HBFP-PEG-PDMS Cross-Linked Terpolymer Networks.** The following general procedure was followed for each sample, as defined here for the terpolymer network having 25 wt % of each PEG and PDMS. To a scintillation vial was added HBFP (100 mg), 1500 Da bis(3-aminopropyl)-terminated PEG (25 mg, 0.017 mmol, 25 wt %), 1500 Da bis(3-aminopropyl)-terminated PDMS (25 mg, 0.010 mmol, 25 wt %), THF (2 mL), and *N,N*-diisopropylethylamine (DIPEA) (0.05 mL, 0.3 mmol), and the mixture was stirred magnetically until homogeneous. The solution was drop cast (0.5 mL per slide) onto precleaned, precut 1 cm<sup>2</sup> glass microscope slides. A period of ca. 30 min allowed for the solvent to evaporate, which afforded a thick pregel that was cured at 110 °C for 45 min under N<sub>2</sub> atmosphere to afford the dry coatings. The cross-linked networks were then characterized prior to and after submersion in a nanopure water bath overnight. The thickness of the films were ca. 0.3 mm for the ATR-IR, static water

contact angle and AFM studies and 1.0 mm for the mechanical analysis studies.

**Preparation of PEG Films for ATR-IR and Surface Force Spectral Mapping.** To a scintillation vial was added bis(3-aminopropyl)-terminated PEG (100 mg, 0.067 mmol), 2,4,6-tris(bromomethyl)mesitylene (18 mg, 0.045 mmol) and THF (1 mL) and stirred until homogeneous. To the solution was added DIPEA (0.12 mL, 0.69 mmol) and stirred for 30 min. The solution was drop cast onto precleaned, precut 1 cm<sup>2</sup> glass coverslips. A period of ca. 30 min allowed for the solvent to evaporate, which afforded a thick pregel that was cured at 110 °C for 45 min under N<sub>2</sub> atmosphere to afford the dry coatings.

**Preparation of PDMS Films for ATR-IR and Surface Force Spectral Mapping.** To a scintillation vial was added bis(3-aminopropyl) terminated PDMS (130 mg, 0.046 mmol), 2,4,6-tris(bromomethyl)mesitylene (12 mg, 0.030 mmol), and THF (1 mL) and stirred until homogeneous. To the solution was added DIPEA (0.09 mL, 0.52 mmol) and stirred for 30 min. The solution was drop cast onto precleaned, precut 1 cm<sup>2</sup> glass coverslips. A period of ca. 30 min allowed for the solvent to evaporate, which afforded a thick pregel that was cured at 110 °C for 45 min under N<sub>2</sub> atmosphere to afford the dry coatings.

## RESULTS AND DISCUSSION

**Synthesis.** A series of three HBFP-PDMS binary networks and nine HBFP-PEG-PDMS terpolymer networks was synthesized with varying stoichiometries of the HBFP, PEG (0, 25, 50, and 75 wt %, relative to HBFP) and PDMS (25, 50, and 75 wt %, relative to HBFP) components, to probe the compositional effects on the physical, mechanical, and biological properties of the cross-linked materials. This process began with the generation of HBFP. Initially, a precursor molecule, **1**, was prepared through a nucleophilic aromatic substitution of 2,3,4,5,6-pentafluorostyrene (PFS) with an excess of tri(ethylene glycol), followed by esterification of the remaining hydroxyl group by reaction with 2-bromopropionyl

bromide to afford the inimer **2** (Scheme 1). Copolymerization of **2** with PFS using CuBr and PMDETA to facilitate atom transfer radical self-condensing vinyl copolymerization was conducted repeatedly to generate batches of HBFP, **3a–c**.<sup>33</sup> The three batches of HBFP were synthesized with only subtle differences in molecular weights, molecular weight distributions, and thermal properties (Supporting Information (SI) Figure S1). Because the three samples of HBFP were of similar composition, structure, and size, each was able to be taken forward individually to create the series of cross-linked bi/terpolymer networks with bis(3-aminopropyl)-terminated PEG and bis(3-aminopropyl)-terminated PDMS, while allowing for direct comparisons to be made regarding the effects of network composition. Significantly lower % Br contents vs the theoretical values were measured by elemental analysis, which is expected to be due to biradical coupling and/or elimination reactions during the copolymerization<sup>34,35</sup> and is being studied in further detail. Nonetheless, stable networks were established, presumably through a cross-linking between the bromoacetyl and bromobenzyl functional handles of the HBFP with the terminal amines of the PEG and PDMS. The networks were generated through deposition on the surface of a microscope slide through solvent casting followed by a thermal cure at 110 °C (Scheme 1). Postcure, the films were submerged in distilled water overnight to extract compounds not bound within the network and release the networks as free-standing, water-swollen films from the substrates.

**Topography and Static Contact Angle.** An initial study probed the terpolymer networks with variation of the HBFP-PEG-PDMS weight percent (wt %) ratios to determine the influence of each component on surface character, as evaluated by AFM and contact angle measurements pre- and postwater immersion (Table 1). In both the dry and wet AFM images, complex topography is seen on the submicrometer scale and surface rearrangement is observed upon water immersion (Table 1). The dynamic reorganization of the surface chemistry during the water immersion was also probed through static water contact angle measurements. The contact angle data of the dry films show an overall decrease in the hydrophobicity of the surface with increasing amounts of PDMS, demonstrating that the HBFP fraction plays an integral role in the surface complexity of the system (SI Figure S2). Upon water immersion, a general decrease in the contact angle is seen in films with 50 wt % PEG or greater, indicating dynamic surface reorganization occurring in these systems and that the PEG-rich regions are discrete enough for isolated regions of water uptake to occur (SI Figure S3). Upon wetting the surfaces having 0 or 25 wt % PEG, an opposite effect was observed, with increases in the static water contact angles. This behavior has been observed for some amphiphilic materials that are capable of dynamic surface reorganization, where PEG-rich hydrophilic regions swell and promote an increase in the fluorocarbon hydrophobic content at the surface, ultimately, resulting in a contraphilic effect, as supported by previous work using secondary ion mass spectrometry (SIMS) and observed in other systems.<sup>31,36</sup>

**Surface Compositional Heterogeneity.** We next focused attention on the one sample composition that gave the most peculiar behavior. Given the generally high surface topographic roughnesses and trends of either increased or decreased water contact angle, for a minority (0 or 25 wt %) vs majority (50 or 75 wt %) of PEG content relative to HBFP, respectively, the one sample that was unique was that having 50 wt % of each

PEG and PDMS, relative to HBFP, which exhibited no change in water contact angle. In order to determine the contribution of the three constituencies to the surface character of the network, surface force spectroscopy (SFS) mapping was performed to differentiate between HBFP-, PDMS-, and PEG-rich regions on the surface of the HBFP-PEG-PDMS terpolymer network with 50 wt % PEG and 50 wt % PDMS (TP). A particular focus was placed on the qualitative differences in surface response as a function of topography. The results of the SFS study are provided as AFM micrographs, spectral maps, and 3D renderings in Figure 1. Surface topography reveals two sets of features, a raised “lattice” of interconnected regions and a lower region interstitial to the “lattice” with a 6.0 nm height differential between the two. However, topography alone reveals little in regards to the innate composition of the two regions and would, in a less complex system, imply a biphasic material. To further our understanding of the surface heterogeneity, SFS was used to determine the relative difference in surface character from feature to feature. Modulus mapping shows that the raised “lattice” is composed of two major variations in response, with islands of higher modulus material connected by lower modulus material. The deeper, interstitial material appears the softest. Deformation mapping at constant force provides an inverse relationship to that observed from modulus mapping, with the stiff island regions deforming 2 nm, the raised portions connecting the island regions deforming 4 nm and the soft, lowered interstitial regions deforming 10 nm at a constant tapping force. Adhesion force mapping provides similar phase information as what might be assumed from topography, while also suggesting that the height of the features may be directly related to the surface energy, where the raised regions are lower energy and the lower regions are rich in higher surface energy material. Dissipation mapping provides information about the energy lost to nonrestorative forces after deformation, and correlates with deformation. From what is known about fluoropolymer, PDMS and PEG surfaces in general, the following assignments are made:

1. HBFP-rich regions. Raised islands with high modulus, low deformation, low surface energy and low dissipation.
2. PDMS-rich regions. Raised “lattice” regions between islands with moderate modulus, moderate deformation, low surface energy and moderate dissipation.
3. PEG-rich regions. Deeper interstitial regions with low modulus, high deformation, high surface energy and high dissipation.

In addition to the study performed on TP, two additional compositions of films were also analyzed using SFS. The three films were tested to determine the difference in their nanomechanical properties at the surface, specifically the compressive moduli of these films. The two additional films chosen were (1) a film that displayed a contraphilic behavior upon wetting, 25 wt % PEG and 25 wt % PDMS, and (2) a film that displayed a normal wetting response, 75 wt % PEG and 75 wt % PDMS. The findings of this study are summarized in SI Table S1. The Young's moduli found at the surfaces were 6.91 MPa, 9.52 MPa, and 11.4 MPa for the 25 wt % PEG and 25 wt % PDMS film, 50 wt % PEG and 50 wt % PDMS film, and 75 wt % PEG and 75 wt % PDMS film, respectively.

**Surface Spectroscopy.** To further support the results of the SFS findings, attenuated total reflectance-infrared spectroscopy (ATR-IR) and X-ray photoelectron spectroscopy (XPS)

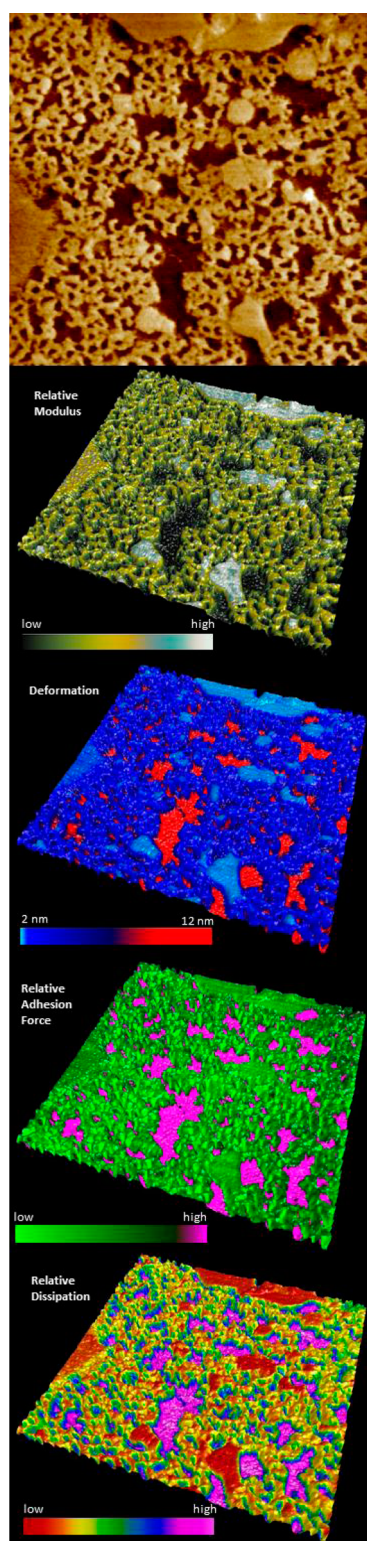


**Figure 1.** Topography and SFS Mapping of TP. Top: AFM micrograph,  $4 \mu\text{m}^2$  field of view. Below: Force spectra transposed on 3D renderings of the topography.

were used to investigate the surface composition of TP. ATR-IR provides IR spectra for the first hundreds of nanometers of the sample network surface, making it a viable method for tracking chemical changes in a polymeric surface.<sup>37</sup> Assessment of the surface of TP pre- and post-water exposure was performed. The assessment was also done for a PDMS and

PEG film and pure HBFP powder. These results are provided in Figure 2. It can be seen that both the PEG and HBFP samples express water signals almost exclusively after swelling. These results are reasonable, as both the PEG coating and the raw HBFP possess glycol domains, which readily uptake water when other constraints do not exist. The PDMS surface displayed only a small water signature, which is also reasonable. Considering the effects on the surface chemistry of the terpolymer system after wetting, several changes become immediately apparent. From comparison to the PEG surface, it can be seen that the PEG contribution to the  $974$  and  $1460 \text{ cm}^{-1}$  signals are greatly diminished after wetting the terpolymer surface. There is also a possibility of diminished PEG in the final system as a result of not fully cross-linking with HBFP, as well as PDMS and HBFP being diminished in the final coating as well. This possible outcome will be analyzed further in the future by characterizing the media in which the film was submerged. It can also be observed that the HBFP signals at  $1497$  and  $1734 \text{ cm}^{-1}$  are expressly present in the terpolymer surface after wetting. Neither of these findings is unique to this system as other HBFP-PEG networks have shown similar behaviors.<sup>31</sup>

The uniqueness of this system is in the gross expression of PDMS character after wetting, where the  $1010 \text{ cm}^{-1}$ ,  $1080 \text{ cm}^{-1}$ , and  $1258 \text{ cm}^{-1}$  PDMS peaks dominate the spectra, thus, making the overall spectra for the terpolymer surface after wetting most closely mimic the PDMS surface spectral signature. The dominance of the PDMS signature is an important result, as it implies that HBFP, in the presence of mobile PDMS after water incubation, does not dominate the surface as in other HBFP-PEG systems. While not necessarily applicable to all the terpolymer systems, this result presents an entirely new method for controlling surface reorganization in these amphiphilic heterogeneous systems via variations in the hydrophilic and hydrophobic components of the HBFP-PEG-PDMS system, opening a full range of surface controls previously unrealized. XPS results clarify that the surface initially possessed all three functionalities in sufficient quantities to have comparable spectral signatures (Figure 2).

**Thermal Response.** TP was investigated by thermogravimetric analysis to determine how cross-linking influences the thermal stability of the network (SI Figure S4). From ambient temperature to  $250 \text{ }^\circ\text{C}$ , 5% mass loss is seen in the network, consistent with a partial degradation of PDMS. There are then two degradation events that can be seen in the network, the first occurring from  $250 \text{ }^\circ\text{C}$  to ca.  $350 \text{ }^\circ\text{C}$  corresponding to a continued degradation of PDMS, and then from  $350$  to  $500 \text{ }^\circ\text{C}$  resulting in an 80% mass loss of the sample in total, corresponding to the decomposition of HBFP and PEG. It can be seen through this study that the cross-links in the system do not infer any additional thermal benefit to the network, but overall, this finding should not detract from the intended uses for this material, under temperatures that vary from  $-2$  to  $33 \text{ }^\circ\text{C}$  and  $36$  to  $38 \text{ }^\circ\text{C}$  for the marine environment and biomedical uses, respectively.

Differential scanning calorimetry was used to probe the phase transitions present in the terpolymer network (SI Figure S5). Upon heating, a melting transition can first be seen at  $33 \text{ }^\circ\text{C}$ , which can be attributed to the PEG in the network, followed by a  $T_g$  at  $63 \text{ }^\circ\text{C}$ , attributed to HBFP.

**Mechanical Response.** *Response under Atmospheric Conditions.* The mechanical properties of TP were investigated with a combination of dynamic mechanical analysis (DMA),



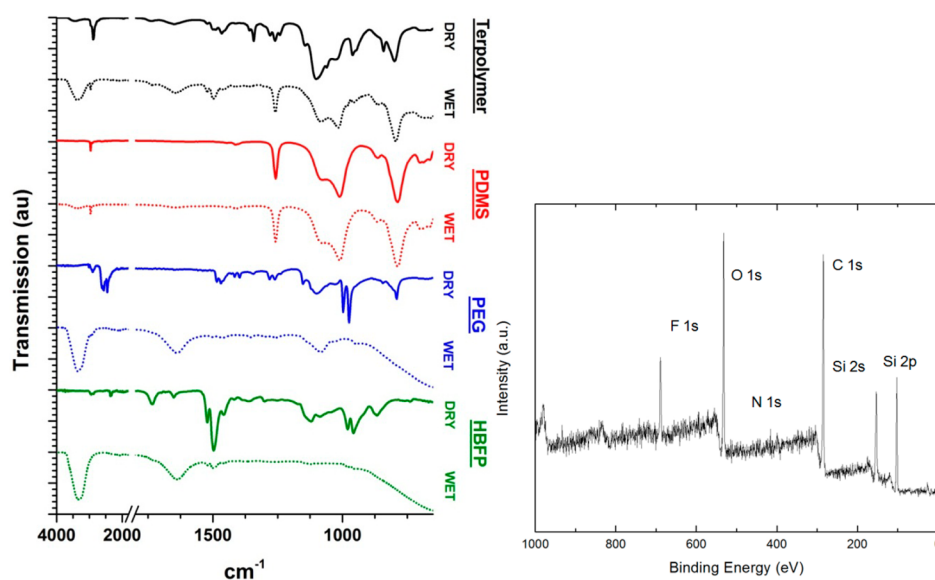


Figure 2. ATR-IR and XPS spectra for TP.

Table 2. Summary of DMA/DTMA with Kinetics

	temp. [°C]	solvent	$E'$ [MPa]	$E''$ [MPa]	$\tan \delta$	time [h]	$\tau$ [h]	notes
A0	25	atmosphere	7.1	1.1	0.158	0		initial
A1	89	atmosphere	10.6	7.5	0.703	1.1		$\tan \delta$ peak
A2	129	atmosphere	1.5	0.39	0.270	1.8		$\tan \delta$ peak
A3	150	atmosphere	0.92	0.16	0.173	2.1		high T ss
M0	20	seawater	10.4	1.6	0.159	0		initial
M1	10	seawater	12.5	2.2	0.178	0.3		
M2	0	seawater	12.8	2.5	0.193	2	$0.07 \pm 0.01$	ss
B0	37	PBS	28.0	4.6	0.164	0		initial
B1	37	PBS	13.1	1.9	0.104	0.1	$0.03 \pm 0.01$	solvation 1
B2	37	PBS	9.8	1.5	0.151	0.4	$0.12 \pm 0.01$	solvation 2
B3	37	PBS	12.5	2.0	0.161	1.7	$0.32 \pm 0.04$	swell
B4	37	PBS	11.7	2.1	0.180	5	$0.61 \pm 0.09$	ss

dynamic thermal mechanical analysis (DTMA) and static stress–strain analysis. Initial investigation of TP by DTMA at 1 Hz (Figure S6) showed two phase transitions via  $\tan \delta$  peaks at 89 (A1) and 129 °C (A2). Room temperature (A0) storage modulus ( $E'$ ) was found to be 7.1 MPa with a loss modulus ( $E''$ ) of 1.1 MPa. A quasi-steady state character was reached near 150 °C (A3), resulting in postphase transition values of 0.92 and 0.16 MPa for  $E'$  and  $E''$ . A frequency sweep at room temperature displayed frequency dependence typical of an amorphous material without significant phase separations or low temperature phase transitions. A summary of DMA and DTMA data can be found in Table 2. Static stress–strain measurements resulted in a characteristic Young's modulus of  $37 \pm 1$  MPa for deformations of less than 1%.

**Response in a Marine Environment.** In order to assess the response in a marine setting, one of the target application environments for these materials, TP was assessed by DTMA in synthetic seawater. The temperature was decreased from 20 (M0) to 0 °C over a 2.5 h period and allowed to equilibrate (M2). The mechanical response of the system over this period is summarized in Table 2, including the  $E'/E''/\tan \delta$  inflection point (M1) observed at 10 °C and the equilibration time constant after reaching 0 °C. Results of this portion of the mechanical assessment are presented in Figure 3 with a plot of the change in  $E'/E''$  per degree change in temperature, as a

function of temperature, to display that at temperatures below 15 °C the effect of temperature on viscosity changes linearly. The ultimate character of TP at 0 °C was a 25% increase in stiffness over initial submersion response and was 50% more resistant to deformation when compared to the ambient condition response in air.

**Response at Physiological Conditions.** This system also has potential application as a coating on biomedical devices, where a decreased likelihood of biomacromolecule or whole cell adhesion is sought. Therefore, assessment of the mechanical response of the TP was performed at conditions that simulate a physiological environment. DMA was performed upon submersion in a pH 7.4 PBS solution at 37 °C (B0), with in situ monitoring to observe solvent uptake (B1 and B2), swelling (B3), and the steady state (B4) response of the film after reaching solvent equilibrium (Figure 4). Two (relatively) fast phases of initial solvent uptake are observed with transition lifetimes of 0.03 and 0.12 h and are assigned to rapid association of the buffer solution with the PEG domains and the hydrophilic regions of the amphiphilic HBFP domains, respectively. These processes resulted in a decrease in  $E'$  of 65%. After initial solvent intercalation into the matrix, a swell period of 1.3 h with a transformation lifetime of 0.32 h occurred before beginning an equilibration process resulting in storage and loss moduli of 12.5 and 2.0 MPa, respectively.

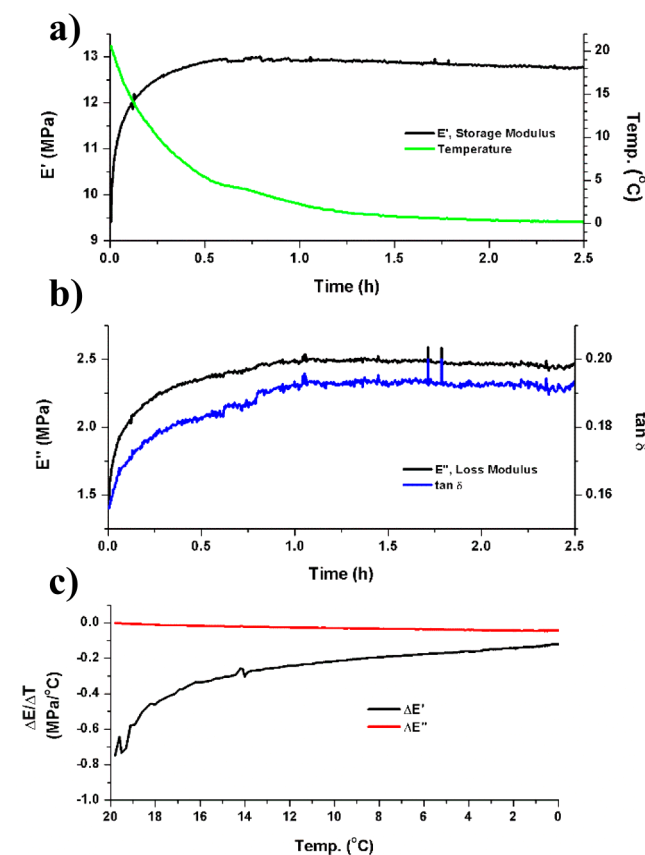


**Figure 3.** Submersion DTMA from 20 to 0  $^{\circ}\text{C}$  in synthetic sea water. (a) Storage modulus and temperature vs time. (b) Loss modulus and  $\tan \delta$  vs time. (c) Total change in modulus per unit change in temperature vs temperature.

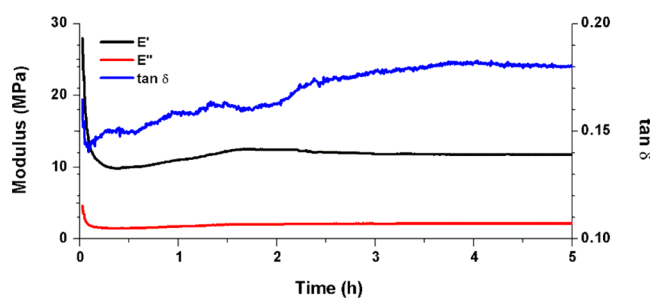


**Figure 4.** Submersion DMA at 37  $^{\circ}\text{C}$  in PBS.

**Nonspecific Protein Resistance.** In an attempt to assess the resistance of the terpolymer network to nonspecific protein binding, an assay was performed using bovine serum albumin (BSA) coupled to Alexa Fluor-680. Both TP and a PDMS standard (Sylgard 184) were evaluated after 45 min of incubation with a 0.1 mg/mL BSA in PBS buffer via confocal fluorescence microscopy. Comparison of the 650 to 750 nm emission histograms of the two surfaces after 635 nm excitation can be found in Figure 5, along with the integrated z-stack images. The change in relative intensities, with identical excitation and collection regimes, shows TP's surface to be ca. 60% less susceptible to BSA adsorption than the standard Sylgard 184 PDMS surface.

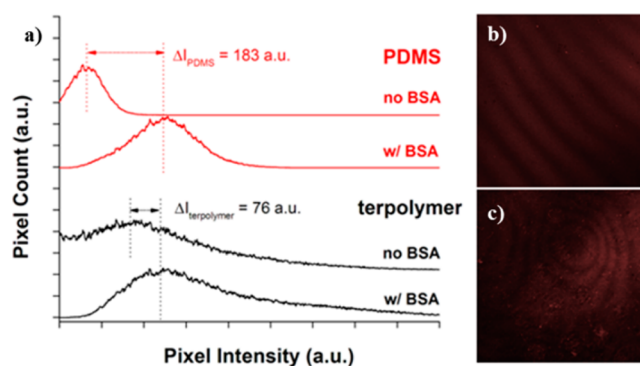


**Figure 5.** Fluorescence signal intensities before and after BSA incubation (left). Confocal micrographs of the PDMS standard (top right) and TP (bottom right) after BSA incubation. Each micrograph is a combined z-stack image of a 10  $\mu\text{m}$  depth field of view taken at 1  $\mu\text{m}$  increments. The  $x$ - $y$  field of view is 2 mm. Excitation occurred via a 635 nm diode laser, with emission collection selected from 650 to 750 nm using a monochromator and a PMT.

## CONCLUSIONS

A series of ternary amphiphilic coatings utilizing HBFP, PEG, and PDMS with unique surface characteristics were synthesized and characterized. It was shown that heterocomplexity and surface energy are explicitly functions of chemical composition and that these systems show promise for use as antibiofouling coatings.

Differing from previous fluoropolymer-PEG systems through incorporation of PDMS, the synthesized terpolymer system expands on the current generation of coatings and displays distinctive topographical, compositional, and morphological features, as seen specifically through analysis of the surfaces by surface force and ATR-IR spectroscopies. The materials presented here provide a direct route to enhanced surface complexity with no significant increase in the synthetic or cure conditions. This system also provides an entirely new mode of dynamic surface reorganization, as shown by preferential emergence of PDMS character on the surface after water immersion, and differing from the predominant fluoropolymer expression observed in previous HBFP-PEG formulations.

By varying the compositional ratios of the three constituents, a wide range of topographical, morphological, and compositional variations were displayed. Microscopic characterization revealed a highly disordered heterogeneous surface that varied both topographically and chemically at the micro- and nanometer-scales. Investigation of nonspecific protein adsorption of the terpolymer network provided encouraging results; with significantly better resistance to protein adsorption than a commercially available antibiofouling PDMS standard. Bulk thermal and mechanical characterization revealed the kinetics and degree of matrix change at both marine and physiological conditions. All of these features provide a new type of amphiphilic surface uniquely qualified for further investigation as a new branch of antibiofouling material.

## ASSOCIATED CONTENT

### Supporting Information

GPC traces of HBFP, contour graphs of static contact angle measurements of dry and wet films, contour graph of the differential static contact angle measurements between dry and water-saturated films, summary of surface force spectroscopy data, TGA traces of TP and each of the homopolymer



components, DSC traces of TP on heating and cooling, DTMA and DMA of in TP in air. This material is available free of charge via the Internet at <http://pubs.acs.org>.

## AUTHOR INFORMATION

### Corresponding Authors

\*E-mail: [jeffery.raymond@chem.tamu.edu](mailto:jeffery.raymond@chem.tamu.edu).

\*Tel: + 1 979 845-4077. Fax: + 1 979 862-1137. E-mail: [wooley@chem.tamu.edu](mailto:wooley@chem.tamu.edu).

### Author Contributions

The manuscript was written through contributions of all authors. All authors have given approval to the final version of the manuscript.

### Notes

The authors declare no competing financial interest.

## ACKNOWLEDGMENTS

This material is based upon work supported by the Office of Naval Research (N00014-10-1-0527 and N00014-14-1-0082). The Welch Foundation is gratefully acknowledged for support through the W. T. Doherty-Welch Chair in Chemistry, Grant No. A-0001. We also thank Dr. Jing Wu of the Materials Characterization Facility at Texas A&M University for her help with the XPS.

## REFERENCES

- (1) Dobretsov, S.; Romani, A. M.; Spratt, D. A.; Ready, D.; Pratten, J. Introduction to Microbial Fouling. In *Biofouling*; Dürr, S., Thomason, J., Eds.; Wiley-Blackwell: West Sussex, 2010; pp 121–122.
- (2) Edyvean, R. Consequences of Fouling on Shipping. In *Biofouling*; Dürr, S., Thomason, J., Eds.; Wiley-Blackwell: West Sussex, 2010; pp 217–225.
- (3) Schultz, M. P.; Bendick, J. A.; Holm, E. R.; Hertel, W. M. Economic Impact of Biofouling on a Naval Surface Ship. *Biofouling* **2010**, *27*, 87–98.
- (4) Dafforn, K. A.; Lewis, J. A.; Johnston, E. L. Antifouling Strategies: History and Regulation, Ecological Impacts, and Mitigation. *Mar. Pollut. Bull.* **2011**, *62*, 453–465.
- (5) Finnie, A. A.; Williams, D. N. Paint and Coatings Technology for the Control of Marine Fouling. In *Biofouling*; Dürr, S., Thomason, J., Eds.; Wiley-Blackwell: West Sussex, 2010; pp 185–206.
- (6) Banerjee, I.; Pangule, R. C.; Kane, R. S. Antifouling Coatings: Recent Developments in the Design of Surfaces That Prevent Fouling by Proteins, Bacteria, and Marine Organisms. *Adv. Mater.* **2011**, *23*, 690–718.
- (7) Grozea, C. M.; Walker, G. C. Approaches in Designing Non-Toxic Polymer Surfaces to Deter Marine Biofouling. *Soft Matter* **2009**, *5*, 4088–4100.
- (8) Gudipati, C. S.; Finlay, J. A.; Callow, J. A.; Callow, M. E.; Wooley, K. L. The Antifouling and Fouling-Release Performance of Hyperbranched Fluoropolymer (HBFP)–Poly(ethylene glycol) (PEG) Composite Coatings Evaluated by Adsorption of Biomacromolecules and the Green Fouling Alga *Ulva*. *Langmuir* **2005**, *21*, 3044–3053.
- (9) Gudipati, C. S.; Greenleaf, C. M.; Johnson, J. A.; Prayongpan, P.; Wooley, K. L. Hyperbranched Fluoropolymer and Linear Poly(ethylene glycol) Based Amphiphilic Crosslinked Networks as Efficient Antifouling Coatings: An Insight into the Surface compositions, Topographies, and Morphologies. *J. Polym. Sci., Part A: Polym. Chem.* **2004**, *42*, 6193–6208.
- (10) Ladd, J.; Zhang, Z.; Chen, S.; Hower, J. C.; Jiang, S. Zwitterionic Polymers Exhibiting High Resistance to Nonspecific Protein Adsorption from Human Serum and Plasma. *Biomacromolecules* **2008**, *9*, 1357–1361.
- (11) Yu, M.; Urban, M. W. Polymeric Surfaces with Anticoagulant, Antifouling, and Antimicrobial Attributes. *Macromol. Symp.* **2009**, *283–284*, 311–318.
- (12) Brady, R. F.; Bonafede, S. J.; Schmidt, D. L. Self-Assembled Water-Borne Fluoropolymer Coatings for Marine Fouling Resistance. *Surf. Coat. Int.* **1999**, *82*, 582–585.
- (13) Feng, S.; Wang, Q.; Gao, Y.; Huang, Y.; Qing, F.-L. Synthesis and Characterization of a Novel Amphiphilic Copolymer Capable as Anti-Biofouling Coating Material. *J. Appl. Polym. Sci.* **2009**, *114*, 2071–2078.
- (14) Webster, D. C.; Chisholm, B. J. New Directions in Antifouling Technology. In *Biofouling*, Dürr, S.; Thomason, J., Eds. Wiley-Blackwell: West Sussex, 2010; pp 366–387.
- (15) Weinman, C. J.; Finlay, J. A.; Park, D.; Paik, M. Y.; Krishnan, S.; Sundaram, H. S.; Dimitriou, M.; Sohn, K. E.; Callow, M. E.; Callow, J. A.; Handlin, D. L.; Willis, C. L.; Kramer, E. J.; Ober, C. K. ABC Triblock Surface Active Block Copolymer with Grafted Ethoxylated Fluoroalkyl Amphiphilic Side Chains for Marine Antifouling/Fouling-Release Applications. *Langmuir* **2009**, *25*, 12266–12274.
- (16) Wang, Y.; Betts, D. E.; Finlay, J. A.; Brewer, L.; Callow, M. E.; Callow, J. A.; Wendt, D. E.; DeSimone, J. M. Photocurable Amphiphilic Perfluoropolyether/Poly(ethylene glycol) Networks for Fouling-Release Coatings. *Macromolecules* **2011**, *44*, 878–885.
- (17) Chisholm, B. J.; Christianson, D. A. Amphiphilic Fouling Release Coatings. U.S. Patent No. US 20120255480, Oct. 11, 2012.
- (18) Yasani, B. R.; Martinelli, E.; Galli, G.; Glisenti, A.; Mieszkin, S.; Callow, M. E.; Callow, J. A. A Comparison between Different Fouling-Release Elastomer Coatings Containing Surface-Active Polymers. *Biofouling* **2014**, *30*, 387–399.
- (19) Bartels, J. W.; Cheng, C.; Powell, K. T.; Xu, J.; Wooley, K. L. Hyperbranched Fluoropolymers and Their Hybridization into Complex Amphiphilic Crosslinked Copolymer Networks. *Macromol. Chem. Phys.* **2007**, *208*, 1676–1687.
- (20) Schumacher, J.; Carman, M.; Estes, T.; Feinberg, A.; Wilson, L.; Callow, M.; Callow, J.; Finlay, J.; Brennan, A. Engineered Antifouling Microtopographies—Effect of Feature Size, Geometry, and Roughness on Settlement of Zoospores of the Green Alga *Ulva*. *Biofouling* **2007**, *23*, 55–62.
- (21) Vaidya, A.; Chaudhury, M. K. Synthesis and Surface Properties of Environmentally Responsive Segmented Polyurethanes. *J. Colloid Interface Sci.* **2002**, *249*, 235–245.
- (22) Hirao, A.; Sugiyama, K.; Yokoyama, H. Precise Synthesis and Surface Structures of Architectural Per- and Semifluorinated Polymers with Well-Defined Structures. *Prog. Polym. Sci.* **2007**, *32*, 1393–1438.
- (23) Andruzzi, L.; Chiellini, E.; Galli, G.; Li, X.; Kang, S. H.; Ober, C. K. Engineering Low Surface Energy Polymers Through Molecular Design: Synthetic Routes to Fluorinated Polystyrene-Based Block Copolymers. *J. Mater. Chem.* **2002**, *12*, 1684–1692.
- (24) Krishnan, S.; Wang, N.; Ober, C. K.; Finlay, J. A.; Callow, M. E.; Callow, J. A.; Hexemer, A.; Sohn, K. E.; Kramer, E. J.; Fischer, D. A. Comparison of the Fouling Release Properties of Hydrophobic Fluorinated and Hydrophilic PEGylated Block Copolymer Surfaces: Attachment Strength of the Diatom *Navicula* and the Green Alga *Ulva*. *Biomacromolecules* **2006**, *7*, 1449–1462.
- (25) Li, X.; Andruzzi, L.; Chiellini, E.; Galli, G.; Ober, C. K.; Hexemer, A.; Kramer, E. J.; Fischer, D. A. Semifluorinated Aromatic Side-Group Polystyrene-Based Block Copolymers: Bulk Structure and Surface Orientation Studies. *Macromolecules* **2002**, *35*, 8078–8087.
- (26) Mueller, A.; Kowalewski, T.; Wooley, K. L. Synthesis, Characterization, and Derivatization of Hyperbranched Polyfluorinated Polymers. *Macromolecules* **1998**, *31*, 776–786.
- (27) Mark James, E. Overview of Siloxane Polymers. In *Silicones and Silicone-Modified Materials*; American Chemical Society: Washington, DC, 2000; Vol. 729, pp 1–10.
- (28) Gasteier, P.; Reska, A.; Schulte, P.; Salber, J.; Offenhäusser, A.; Moeller, M.; Groll, J. Surface Grafting of PEO-Based Star-Shaped Molecules for Bioanalytical and Biomedical Applications. *Macromol. Biosci.* **2007**, *7*, 1010–1023.
- (29) Ekblad, T.; Bergström, G.; Ederth, T.; Conlan, S. L.; Mutton, R.; Clare, A. S.; Wang, S.; Liu, Y.; Zhao, Q.; D'Souza, F.; Donnelly, G. T.; Willemsen, P. R.; Pettitt, M. E.; Callow, M. E.; Callow, J. A.; Liedberg, B. Poly(ethylene glycol)-Containing Hydrogel Surfaces for Antifouling

Applications in Marine and Freshwater Environments. *Biomacromolecules* **2008**, *9*, 2775–2783.

(30) Gan, D.; Mueller, A.; Wooley, K. L. Amphiphilic and Hydrophobic Surface Patterns Generated from Hyperbranched Fluoropolymer/Linear Polymer Networks: Minimally Adhesive Coatings via the Crosslinking of Hyperbranched Fluoropolymers. *J. Polym. Sci., Part A: Polym. Chem.* **2003**, *41*, 3531–3540.

(31) Imbesi, P. M.; Finlay, J. A.; Aldred, N.; Eller, M. J.; Felder, S. E.; Pollack, K. A.; Lonnecker, A. T.; Raymond, J. E.; Mackay, M. E.; Schweikert, E. A.; Clare, A. S.; Callow, J. A.; Callow, M. E.; Wooley, K. L. Targeted Surface Nanocomplexity: Two-Dimensional Control over the Composition, Physical Properties and Anti-Biofouling Performance of Hyperbranched Fluoropolymer-Poly(ethylene glycol) Amphiphilic Crosslinked Networks. *Polym. Chem.* **2012**, *3*, 3121–3131.

(32) Neumann, A. W.; Good, R. J. *Techniques of Measuring Contact Angles*; Plenum Press: New York, 1979; Vol. 11.

(33) Powell, K. T.; Cheng, C.; Wooley, K. L. Complex Amphiphilic Hyperbranched Fluoropolymers by Atom Transfer Radical Self-Condensing Vinyl (Co)polymerization. *Macromolecules* **2007**, *40*, 4509–4515.

(34) Lutz, J.-F.; Matyjaszewski, K. Nuclear Magnetic Resonance Monitoring of Chain-End Functionality in the Atom Transfer Radical Polymerization of Styrene. *J. Polym. Sci., Part A: Polym. Chem.* **2005**, *43*, 897–910.

(35) Cheng, C.; Wooley, K. L.; Khoshdel, E. Hyperbranched Fluorocopolymers by Atom Transfer Radical Self-condensing Vinyl Copolymerization. *J. Polym. Sci., Part A: Polym. Chem.* **2005**, *43*, 4754–4770.

(36) Makal, U.; Uslu, N.; Wynne, K. J. Water Makes It Hydrophobic: Contraphilic Wetting for Polyurethanes with Soft Blocks Having Semifluorinated and 5,5-Dimethylhydantoin Side Chains. *Langmuir* **2006**, *23*, 209–216.

(37) Mirabella, F. M., Jr. *Practical Spectroscopy Series: Internal Reflection Spectroscopy: Theory and Applications*; Marcel Dekker, Inc.: New York, 1993; pp 17–52.